Molecular Dynamics Simulation of Thermomechanical Properties of Montmorillonite Crystal. II. Hydrated Montmorillonite Crystal

ARTICLE *in* THE JOURNAL OF PHYSICAL CHEMISTRY C · OCTOBER 2008

Impact Factor: 4.77 · DOI: 10.1021/jp711188u

6 AUTHORS, INCLUDING:

Mikhail Abramovich Mazo
Semenov Institute of Chemical Physics
50 PUBLICATIONS **334** CITATIONS
SEE PROFILE

Alexander Alexandrovich Berlin
Russian Academy of Sciences
399 PUBLICATIONS **716** CITATIONS
SEE PROFILE

Nikolay K. Balabaev
Russian Academy of Sciences
133 PUBLICATIONS **948** CITATIONS
SEE PROFILE

Molecular Dynamics Simulation of Thermomechanical Properties of Montmorillonite Crystal. II. Hydrated Montmorillonite Crystal

Mikhail A. Mazo,[†,*] Leonid I. Manevitch,[†] Elena B. Gusarova,[†] Alexander A. Berlin,[†] Nikolay K. Balabaev,[‡] and Gregory C. Rutledge[§]

Semenov Institute of Chemical Physics, Russian Academy of Science, Kosygin str. 4, Moscow, 119991, Russia, Institute of Mathematical Problems of Biology, Russian Academy of Science, Pushchino, 142290 Russia, and Department of Chemical Engineering, Massachusetts Institute of Technology, Cambridge, Massachusetts 02139

Received: November 26, 2007; Revised Manuscript Received: August 19, 2008

We present the results of molecular dynamics simulation of the thermomechanical behavior of Wyoming-type Na^+-montmorillonite (MMT) with water intercalates. Montmorillonite is commonly used as a filler in polymer−clay nanocomposites, and calculation of the elastic properties of the composite requires accurate knowledge of the elastic moduli and thermal properties of the components. To calculate the properties of the filler, we used a computational cell containing two MMT lamellae $[Si_{248}Al_8][Al_{112}Mg_{16}]O_{640}[OH]_{128}$ and periodic boundary conditions in all three directions. The galleries between each pair of MMT lamella were filled with 24 Na^+ counterions and either one or two water layers (100 and 200 mg/g clay, respectively). The results obtained for the interlayer distance and the number density profiles of water molecules and Na^+ ions in galleries are in good agreement with experimental data and results of other computer simulations. The thermal properties were analyzed over the range of 300−400 K; the isothermal linear compressibility and all of the components of the elasticity tensor were calculated. It turns out that the elasticity tensor possesses orthotropic symmetry and changes very weakly with temperature in the range 300−350 K. The calculated in-plane Young's moduli of the hydrated MMT are equal at 180 GPa for the case of an intercalated monolayer of water and 150 GPa for that of an intercalated bilayer of water. The shear moduli parallel to the lamellae decrease from 20 GPa for the monolayer case to 2−4 GPa for the bilayer case. The water interlayer significantly alters the linear coefficient of thermal expansion and Young's modulus perpendicular to the clay lamellae in the hydrated crystal. In the monolayer case, the linear coefficient of thermal expansion $K_{T,Z}$ was only slightly larger than that for pyrophyllite but increased noticeably in the bilayer case.

1. Introduction

In recent years, swollen clay minerals have attracted interest not only because of their importance for the earth sciences but also their significant role in many industrial applications, such as petroleum engineering, civil engineering, food and cosmetic industry, heterogeneous catalysis, waste storage, etc. Special interest in these minerals appeared after it was disclosed that nanoclay fillers can improve significantly the mechanical and thermal properties of polymer composites and decrease their permeability, which influences their biodegradation in biomedical applications.[1−4] Such "nanocomposites" are now used as barrier films in packaging, as fire retardant coatings, in aerospace and automotive parts, etc., and have potential applications in aviation, medicine, and other industries.

Swollen clay minerals consist of negatively charged crystal sheets and water molecule hydrates with charge-compensating cations in the interlayer space between sheets, called "galleries".[5] In particular, aluminum phyllosilicate montmorillonite (MMT), one of the most commonly used smectites, is composed of two silicate tetrahedral sheets sandwiching one aluminum−oxygen−hydroxyl octahedral sheet; some aluminum atoms in the octahedral sheet are substituted by magnesium atoms, and some silica atoms are replaced by aluminum atoms. As a result, the aluminosilicate sheets of MMT are negatively charged and held together by cations. A characteristic property of these crystals is their ability to adsorb water into the galleries, resulting in strong repulsive forces and swelling of the clay.

Computer simulations provide an important means for understanding the physicochemical processes in the water−clay systems at the microscopic level and for the interpretation of experimental results. The first model of hydrated MMT and vermiculite crystals, proposed by Skipper et al.,[6,7] already showed that computer simulations can be used for the structural analysis of water and different ions between the clay plates. Later, molecular dynamics (MD) and Monte Carlo (MC) simulations were extensively applied to the analysis of swelling of the MMT[8−39] and another aluminum phyllosilicates.[40−45]

It was found in earlier experiments that swelling occurs through several distinct steps, forming one-, two-, and three-layer hydrates.[5] Computer simulation allowed to reproduce the swelling curves[10−13,20,25] and to obtain unique information about the molecular structure of these layers[7−21,25−30,44] and its dependence on the type of cations.[11,14,17−22,24,29−32] In addition, the free energy and entropy of clay mineral swelling,[16,29,30] as well as the influence of temperature[36] and pressure[36,41] on the swelling, were calculated. Water adsorption isotherms[22,29] and smectite−water interactions at geothermal and geostatic gradients up to a depth of several kilometers[13] were simultaneously

* To whom correspondence should be addressed. Fax: (7495)-137-8284. E-mail: mazo@polymer.chph.ras.ru.
† Semenov Institute of Chemical Physics, Russian Academy of Science.
‡ Institute of Mathematical Problems of Biology, Russian Academy of Science.
§ Massachusetts Institute of Technology.

10.1021/jp711188u CCC: $40.75
Published on Web 10/10/2008

calculated, and the isothermal compressibility of the water layer was estimated from volume fluctuations.[11]

Despite that attention given to the mobility of water molecules and ions in the clay minerals,[10,16,24−28,33,37−39] numerous questions regarding the state of water molecules in the intercalated mono- and bilayers of water remain. Ichikawa et al.[16,27,28] observed a dramatic decrease in the self-diffusion coefficient of water D_w and an increase in the shear viscosity in the vicinity of the lamellae of Na-MMT (the "iceberg effect"). The same result was obtained by Leng and Cummings[42,43] for muscovite, where intercalated monolayers and bilayers of water are frozen at 298 K. On the other hand, using ^{2}H NMR spectroscopy and computer simulation Porion et al.[39] found that water molecules adsorbed in the interlamellar space of MMT in monohydrated systems are rather mobile, with their self-diffusion coefficient D_w ($D_w \approx 2 \times 10^{-10}$ m^2 s^{-1}) being only 1 order of magnitude less than that of bulk water[46] ($D_w = 23 \times 10^{-10}$ m^2 s^{-1}). Malikova et al.[33,37] studied the diffusion coefficients of water molecules in an intercalated bilayer for Na-MMT and Cs-MMT as a function of temperature in computer simulation and by quasielastic neutron scattering and neutron spin echo techniques. They also concluded that water molecules within the bilayer have a self-diffusion coefficient of the same order of magnitude as in bulk water ($D_w = 10-15 \times 10^{-10}$ m^2 s^{-1}).

Most of the above-mentioned works[6−15,17−26,29,33,36,37] were based on the model of Skipper et al.[6] and used a rigid clay lattice. Those authors believed that the rigid-lattice approximation had little effect on calculated properties, and therefore the use of such models was justified by computational efficiency. However, the rigid lattice can noticeably affect the dynamical properties, in particular, the diffusion properties of the gallery contents. Moreover, this restriction on the clay lamella is unsuitable for the study of the temperature dependence of mineral structures, the vibrational spectra and mechanical properties of the clay.

Kawamura et al. were the first to elaborate the atom pair potentials for molecular dynamics simulations of structural and dynamical properties of aluminosilicates.[47] This force field included the Coulomb interaction, the short-range repulsion, and the van der Waals and Morse terms. A three-body term was added for the H−O−H interaction for both covalent and hydrogen bonds. Later, Ichikawa et al. used these potentials to study molecular behavior of MMT hydrate in pure and salt water.[16,27,28] Hill and Sauer proposed molecular potentials for MD simulation of aluminosilicates on the basis of the consistent force field (CFF).[48,49] Teppen et al. developed these covalent-type potentials to carry out the simulation of gibbsite, kaolinite, pyrophyllite, and beidellite.[50] Later, this force field was used for the study of adsorption of well-defined organic molecules[51] to aluminosilicate surfaces, as well as to evaluate the deformation response to stress of pyrophyllite in the dry state and of MMT in the dry state and hydrated states with one, two, and three layers of water.[34,35] The deformations of the clay lamellae and interlamellar water were studied under high loads (2.5−3 GPa) applied normal to the clay lamellae at 300 K. Earlier, we also used this force field to study the mechanical properties of a single lamella of MMT at room temperature.[52]

Recently, Cygan et al. developed a new force field (CLAYFF) taking into account that metal atoms and, to some extent, oxygen atoms possess ionic form.[53] The interatomic interactions in CLAYFF consist solely of electrostatic and Lennard-Jones terms except for the O−H bond, which is constrained by a harmonic bond stretch potential. This force field has been shown to be highly effective in modeling the crystal structure of a number of different clays,[38,39,41,42,53] mobility of interlayer water,[38,39,41,42,45] for studying the structure, dynamics, and energetics of cement materials,[54] and the vibrational spectrum of hydrotalcite,[53] brucite,[55] and pyrophyllite.[56] Recently Suter et al. simulated the deformation of MMT with a water monolayer and calculated the in-plane elasticity coefficients and bending modulus at 300 K using large-scale atomistic simulations and the CLAYFF force field.[38]

Earlier, we reported the elastic and thermal properties of an isolated pyrophyllite lamella[57] and of MMT with poly(ethylene oxide) oligomer intercalates[58] at different temperatures using the CLAYFF force field. In this paper, we calculate the elastic and thermal properties of a Na^+-MMT crystal with mono- and bilayers of water at 300 and 350 K. The paper is organized as follows: in the next section, we describe the model, the force field used, and the details of the MD simulations. We present also the parameters of the equilibrium structure of our model: the dimensions of calculated cells, the interlayer distance d, and the number density profiles of water molecules and Na^+ cations in galleries at 300 and 350 K. In section 3, we investigate the coefficients of thermal expansion (CTE) of the hydrated MMT crystal. In section 4, we present the result of calculation of the components of the elasticity tensor of the hydrated MMT. In section 5, we briefly discuss the thermo-mechanical properties of the water−ion layers in the transverse direction. In the Conclusion, we summarize the main results of the investigation.

2. Model and Simulation Details

The system under consideration is a fully atomistic model of Na^+-MMT with intercalated water. We used an oblique parallelepiped computational cell with periodic boundary conditions in all three directions. The cell contained two Wyoming-type MMT lamellae $[Si_{248}Al_8][Al_{112}Mg_{16}]O_{640}[OH]_{128}$ oriented parallel to the XY plane. The atomic structure of the unit cell of montmorillonite was taken from X-ray diffraction measurements of pyrophyllite.[59] One of eight aluminum atoms in the octahedral sheet was substituted by a magnesium atom, and one of 32 silica atoms in the tetrahedral sheets was replaced by an aluminum atom according to a previous study,[20] after which the unit cell was replicated 8 times in the Y direction (a axis) and 4 times in the X direction (b axis).

The space between the MMT lamellae (two clay galleries) was filled by 24 counterions of Na^+ and 128 or 256 water molecules (corresponding to water content of 100 and 200 mg/g clay, respectively). The number of water molecules in the interlamellar galleries conform to the results of previous works[11,20] and correspond to a plateau in the dependence of the interlamellar distance on water concentration.

We used a computational cell with variable box shape. The initial cuboid-shaped cells had dimensions 3.6 × 4.2 × 2.5 nm ($L_x \times L_y \times L_z$) for the system with monolayers of water and 3.6 × 4.2 × 2.9 nm for the system with bilayers of water (Figure 1). Water molecules have been described by a flexible version[60] of the TIP3P potential model.[61] We employed the empirical CLAYFF force field[53] and screened Coulombic interactions while calculating electrostatic energy U_{ij} between atoms i and j

$$U_{ij}(r_{ij}) = \frac{q_i q_j}{\varepsilon r_{ij}} W(r_{ij})$$

$$W(r_{ij}) = \begin{cases} (1 - r_{ij}/R_{\text{off}})^2; & r_{ij} < R_{\text{off}} \\ 0; & r_{ij} \geq R_{\text{off}} \end{cases}$$

where q_i and q_j represent the charges on the ith and jth atoms, r_{ij} the distance between them, and R_{off} is a cutoff radius. We

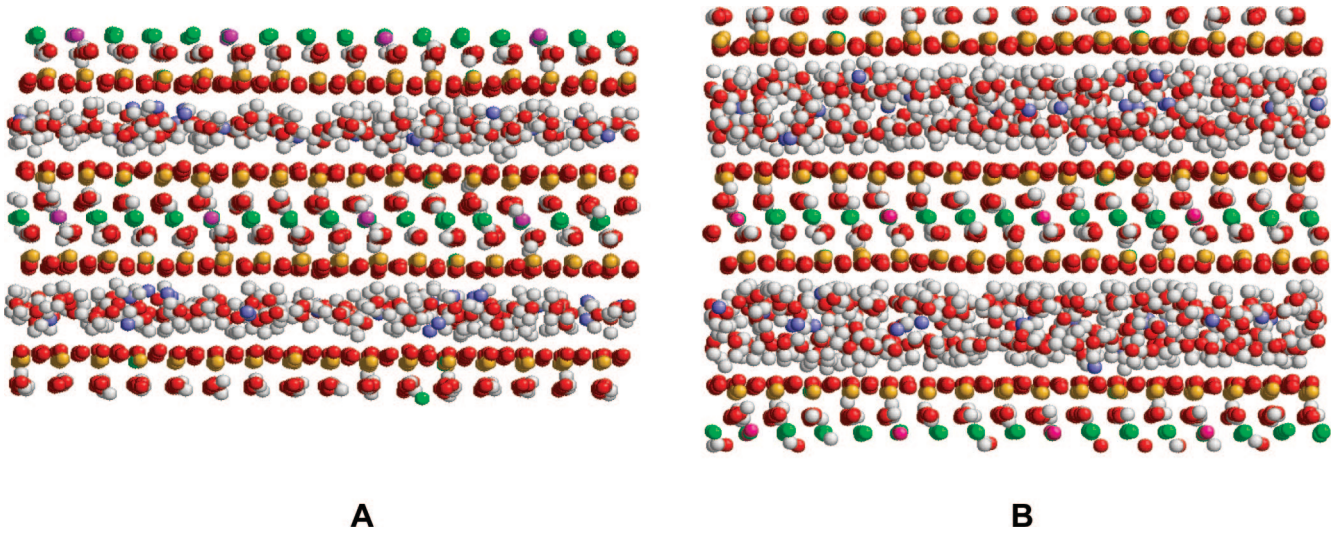

Figure 1. The samples of MMT crystal with Na^+ counterions and monolayers (A) or bilayers (B) of water between the clay plates. The atoms are colored as follows: Si, yellow; O, red; H, white; Al, green; Na, blue; Mg, magenta.

TABLE 1: Layer Spacing *d* for Hydrated MMT with a Monolayer and Bilayer of Water (100 and 200 mg/g Clay, Respectively)

	water monolayer	water bilayer
this work, computer simulation	1.2300 ± 0.0005	1.4745 ± 0.0005
Marry et al., computer simulation[25]	1.23	1.53
Suter et al., computer simulation[38]	1.2051 ± 0.005	NA
Fu et al., experimental data[64]	1.23	1.5
Calvet, experimental data[66]	1.25	NA

took the cutoff radius equal to 1.05 nm for van der Waals interactions and to 1.25 nm for Coulombic interactions. Additional calculations have shown that the results turn out to be practically independent of the cutoff radius of Coulombic interactions 1.25, 1.5, and 1.8 nm. The system evolved according to Newton's equations of motion with additional terms providing for the Berendsen barostat[62] and collisional thermostat.[63] An additional constraint was applied to fix the position of the center of mass of the system, thereby preventing translational displacement of the system as a whole. The equations of motion were integrated using the velocity Verlet algorithm[64] with an integration step 0.5 fs.

The initial equilibrium state of the confined water molecules was determined by MD simulations. After that we performed the MD calculations using the NVT ensemble at high temperature, 800 K, for 100 ps. Next, the system was quenched to the desired temperature (300 or 350 K) and pressure (1 atm) and equilibrated over a period of 500 ps. The sizes of clay unit cell obtained at 300 K ($a = 0.5194 \pm 1 \times 10^{-4}$ nm and $b = 0.8978 \pm 1 \times 10^{-4}$ nm) are in good agreement with experimental[5,65−67] and simulation[38,52,53] data. The calculated layer spacing *d* conforms to experimental and simulation data as well (Table 1).

The number density profiles of water molecules and Na^+ cations in the galleries (Figure 2) are in agreement with the available experimental data[14] and results of computer simulation.[20,26,29,30] The peaks corresponding to the oxygen atoms of the water molecules indicate that these are organized in one or two layers in the interlamellar space. The distribution of water hydrogens in the monolayer has a symmetric, three-peak structure, with a maximum at the center of the gallery. The sodium ions are distributed around the water oxygens. The distribution of water hydrogens in the bilayer has a symmetric, five-peak structure, and the ions are preferentially concentrated at the center of the gallery and have a three-peak structure. The increase in temperature from 300 to 350 K does not affect the structure of the interlamellar contents. Thus, the results obtained, being in good accordance with the known ones, confirm the reliability of our model.

3. Calculation of the Thermal Expansion

The thermal properties were analyzed in the range of 300−400 K. For this purpose we increased and decreased the temperature at a constant rate of 1.0 and 0.5 K/ps in this temperature range during the computer simulations. We performed 4−5 cycles of heating and cooling for every sample,

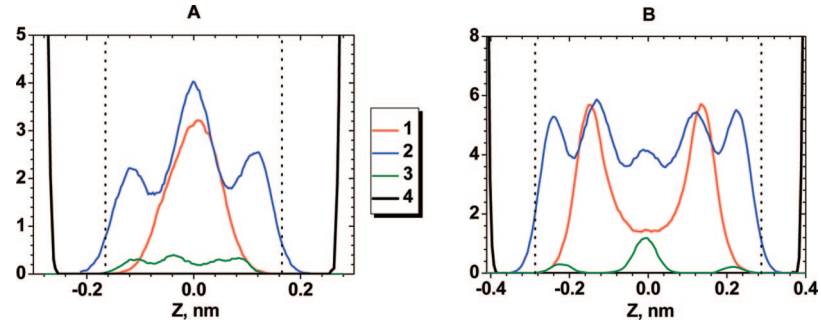

Figure 2. The number density profiles of water molecules and Na^+ cations in the galleries perpendicular to the clay lamellae at 300 K: water monolayer (A) and water bilayer (B). Black, the clay oxygen atoms; blue, water hydrogen; red, water oxygen; green, sodium ion. Dotted lines denote the boundaries between clay lamella and water layer.

TABLE 2: Calculated Linear ($K_{T,a}$, $K_{T,b}$, $K_{T,Z}$) and Volume ($K_{T,V}$) Coefficients of Thermal Expansion of Hydrated MMT crystal ($\times 10^{-5}$ K^{-1})

	$K_{T,a}$	$K_{T,b}$	$K_{T,Z}$	$K_{T,V}$
single pyrophyllite lamella	1.01 ± 0.01	1.03 ± 0.01	1.01 ± 0.03[a]	3.14 ± 0.04
MMT with a monolayer of water	0.92 ± 0.1	1.2 ± 0.1	1.47 ± 0.05	3.5 ± 0.1
MMT with a bilayer of water	1.09 ± 0.1	1.3 ± 0.1	3.01 ± 0.05	5.5 ± 0.1

[a] Taking into account the van der Waals atomic radii, which increase the effective thickness of the clay plate from 0.6425 to 0.98 nm.[52,67]

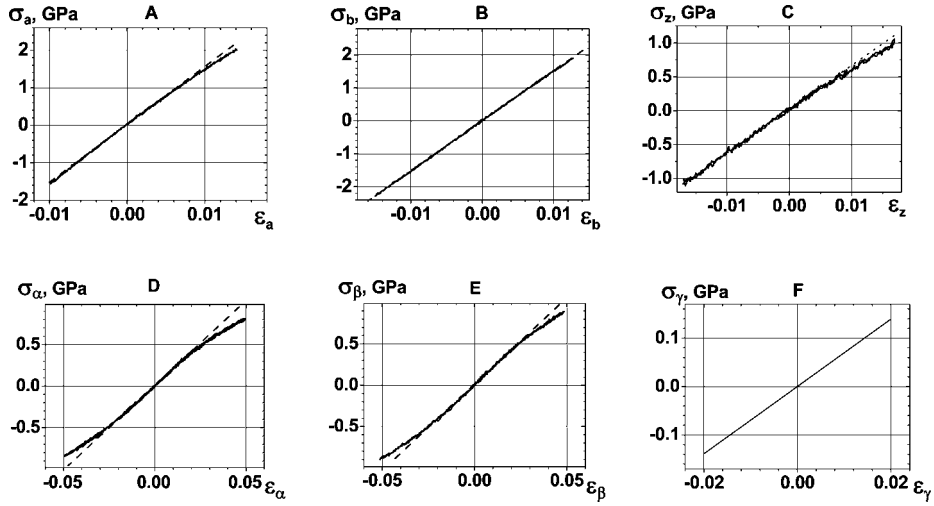

Figure 3. Typical stress−strain behavior for a hydrated MMT crystal with a water monolayer at 300 K: uniaxial deformations along *a* axis (A), *b* axis (B), and *z* direction (C) as well as pure shear in the *XZ* plane (D), in the *YZ* plane (E), and in the *XY* plane (F).

keeping the pressure at 1 atm. The sizes of the calculation cell in these runs were reproducible with good accuracy and allowed us to calculate the linear ($K_{T,a}$, $K_{T,b}$, $K_{T,Z}$) and volume ($K_{T,V}$) coefficients of thermal expansion for the hydrated MMT crystals with either a monolayer or bilayer of water.

As expected, the temperature dependence of the composite in the *XY* plane was determined primarily by the linear CTEs of the clay lamella and does not depend on the number of water layers; it accords well with our previous results for pyrophyllite[57] (Table 2). We observed only a small increase in $K_{T,b}$ for hydrated MMT, which can probably be traced to the difference between the structures of the pyrophyllite and montmorillonite lamellae or to the influence of the water interlayer. On the contrary, the water layers influence dramatically the linear CTE in the *Z* direction. While $K_{T,Z}$ in the case of a water monolayer was only slightly larger than that for pyrophyllite, it was significantly larger in the case of the water bilayer.

4. Calculation of the Components of Elasticity Tensor

To calculate the elastic properties of the hydrated MMT crystal, we deformed our calculation cell with constant strain rate, as described earlier.[57] By use of the oblique parallelepiped computational cell, we carried out six different deformations: three uniaxial deformations along the crystallographic axes *a*, *b*, and *c*, by changing the corresponding dimension of the computational cell, and three pure shear deformations, by changing the corresponding angle of the computational cell α, β, and γ (hereinafter we denote them by indexes 1, 2, 3, 4, 5, and 6, respectively). By use of Voigt notation,[67] in accordance with Hooke's law for deformation in the *n*th direction one can write

$$\varepsilon_i^{(n)} = \sum_j S_{ij}\sigma_j^{(n)} \quad n = 1, 2, 6 \qquad (1)$$

where $\varepsilon_i^{(n)}$ and $\sigma_j^{(n)}$ are the components of strain and stress, respectively, and the $\mathbf{S}_{ij}$ are the components of the compliance tensor in the 6×6 symmetric matrix, also in Voigt form. In our simulation we specified $\varepsilon_n^{(n)}$, providing $\sigma_j^{(n)} = 0$ for $j \neq n$ and measured the values $\sigma_n^{(n)}$ and $\varepsilon_i^{(n)}$ for $i \neq n$, which allowed to calculate all components of the matrix S_{ij} from eq 1 without any suppositions regarding its symmetry: $\mathbf{S}_{ij} = \varepsilon_i^{(j)}/\sigma_j^{(j)}$.

We realized all deformations using a constant strain rate. Two different rates of deformation (0.06 and 0.12 ns^{-1} during uniaxial deformation and 0.25 and 0.5 rad ns^{-1} during shear deformation) were used, but the results of calculations were found not to depend on the deformation rate in these ranges. Each run contained 2−4 complete cycles of extension and compression or shear in opposing directions. The maximum strain amplitude was 1−2% for uniaxial deformation and 5% for shear deformations. The temperature was held constant at 300 or 350 K. Characteristic examples of calculated relationships such as shear stress vs shear strain are shown in Figure 3. From the components of the compliance tensor obtained by eq 1, we determined the Young's moduli $\mathbf{E}_i = 1/\mathbf{S}_{ii}$, Poisson coefficients $\nu_{ij} = \varepsilon_i^j/\varepsilon_j^j$, and the components of the elasticity tensor $\mathbf{C}_{ij} = \mathbf{S}_{ij}^{-1}$ for hydrated MMT with monolayers or bilayers of water. It turns out that mechanical properties are practically invariable in the temperature range under study. Therefore we discuss the results for 300 K only.

Because the matrices $\mathbf{S}_{ij}$ and $\mathbf{C}_{ij}$ have to be symmetric, their symmetry is a good test of the accuracy of the calculations. As can be seen from Tables 3 and 4, the stiffness matrixes $\mathbf{C}_{ij}$ for both monolayers and bilayers are symmetric with good accuracy. Furthermore, the $\mathbf{C}_{ij}$ matrices exhibit nearly orthotropic symmetry, in accord with the supposition of Suter et al.[39] The calculated elastic constants (in GPa) and Poisson ratios for the hydrated MMT crystals with monolayers or bilayers of water are presented in Table 5; the results obtained by Suter et al.[38] are also shown for comparison.

Increasing the interlamellar water film thickness within the galleries from a monolayer to a bilayer leads to an increase of the interlamellar distance and, as a consequence, to a corre-

TABLE 3: Components of the Elasticity Tensor C_{ik} of MMT with Water Monolayers in GPa at 300 K

i/*k*	1	2	3	4	5	6
1, *Y* axis	**231**	105	17	−3	2	0
2, *X* axis	103	**229**	15	3	4	0
3, *Z* axis	16	15	**80**	0	2	0
4, angle α	−3	5	0	**21**	1	2
5, angle β	1	2	−2	0	**22**	−3
6, angle γ	0	0	0	2	−4	**68**

TABLE 4: Components of the Elasticity Tensor C_{ik} of MMT with Water Bilayers in GPa at 300 K

i/*k*	1	2	3	4	5	6
1, *Y* axis	**189**	84	6	0	0	0
2, *X* axis	87	**191**	5	0	0	0
3, *Z* axis	6	6	62	0	0	0
4, angle α	1	1	−1	**2**	0	0
5, angle β	1	0	0	0	4	0
6, angle γ	0	0	0	0	0	**56**

TABLE 5: Elastic Constants (in GPa) and Poisson Ratios of the Elasticity Tensor Components Calculated for the Hydrated MMT Crystal

	our calculations		Suter et al.[38]
	monolayer	bilayer	monolayer
E_1	182 ± 1	150 ± 1	182
E_2	180 ± 1	152 ± 1	172
E_3	78.1 ± 0.1	61.7 ± 0.1	
E_4	20.4 ± 0.1	2.3 ± 0.1	
E_5	19.0 ± 0.1	4.0 ± 0.1	
E_6	66.7 ± 0.1	56.5 ± 0.1	
ν_{12}	0.45 ± 0.01	0.44 ± 0.01	0.36
ν_{21}	0.44 ± 0.01	0.46 ± 0.01	0.36
ν_{13}	0.12 ± 0.02	0.06 ± 0.02	0.17
ν_{31}	0.05 ± 0.02	0.02 ± 0.02	
ν_{23}	0.10 ± 0.01	0.04 ± 0.02	
ν_{32}	0.04 ± 0.02	0.02 ± 0.02	0.17

sponding decrease in stiffness of about 17% for our case. The interlamellar water affects the Young's modulus of the crystal in the transverse direction and the transverse shear stiffnesses the most, reducing E_3 by 21% but E_4 and E_5 severalfold. Nevertheless, even in this case E_4 and E_5 remain nonzero. This observation suggests that the interlamellar water-cation film is more solidlike than liquidlike on the time scale of these computer experiments. By use of the CFF force field,[50] Katti et al. obtained a basal spacing modulus of considerably lower magnitude in the linear region of deformation: 14.5 GPa for the water monolayer and 1.4 GPa for the water bilayer.[34,35] This discrepancy probably results from differences in the water models used and from the slightly different MMT structure used by Katti et al. ($NaSi_{16}(Al_6FeMg)O_{40}(OH)_8$), in which the surface charge is less than in our model system.

The in-plane elastic constants of the hydrated MMT crystal depend mainly on the lamellar stiffness. As one can see from Table 5, good agreement is observed between the values of E_1 and E_2 obtained by us for the case of a water monolayer and those previously reported by Suter et al.[38] However, in contrast to our calculation, they observed slightly lower magnitudes of E_2 and Poisson ratios ν_{12} and ν_{21}. The discrepancy could arise due to the different structure of the lamellae (different distribution of the tetrahedral aluminum and octahedral magnesium) simulated or differences in the parameters of the water model used.

5. Thermomechanical Properties of the Water−Ion Layers

Up to now, we have discussed the effect of the interlamellar layer on thermal and mechanical properties of the hydrated MMT crystal. But what are the properties of the water−cation interlamellar layer itself? Invoking simple series and parallel models for parallel sheets of clay lamellae and water films, the CTE, the coefficient of isothermal compressibility, and the mechanical properties in the hydrated MMT crystal model can be related to the appropriate properties in the individual clay lamellae and water films. In particular, we have for the linear CTEs ($K_{T,Z}$) and the coefficients of isothermal compressibility β_Z in the *Z* direction

$$dK^{M}_{T,Z} = h_w K^{w}_{T,Z} + h_l K^{l}_{T,Z}$$
$$d\beta^{M}_{Z} = h_w \beta^{w}_{Z} + h_l \beta^{l}_{Z} \quad (2)$$

where the superscripts M, w, and l refer to the hydrated MMT crystal, the interlamellar water layer, and the clay lamella, respectively; *d* is the layer spacing; h_l and h_w are the thicknesses of the interlamellar water layer and the clay lamella, respectively, such that $d = h_l + h_w$. There is some ambiguity in the estimation of the magnitudes of h_l.[52,57,69] Here we calculated properties of the water layer and the clay lamella for three values of h_l: 0.6425, 0.90, and 0.98 nm. The former value was obtained for pyrophyllite lamella[57] when the lamella boundary coincided with a plane of oxygen atoms at the lamella surface. That value is useful for calculation of mechanical properties of an isolated lamella but does not take into account the atomic size. To keep in mind the van der Waals radius of atoms it was suggested to consider the values 0.96[52] and 0.98 nm.[58,69] We can also consider the center of the space between the lamella surface oxygen and the water oxygen as the boundary of lamella and water as well as in,[34,35] that seemingly more preferably. In this case h_l is equal 0.9 nm (Figure 2).

The calculated magnitudes of the linear CTEs of the films ($K^{w}_{T,Z}$) and experimental data for water in bulk[70] are presented in Table 6. One can see that the CTE of the monolayer film for all h_l is several times smaller than that of the bulk; the CTE of the bilayer is intermediate between the values of the monolayer and bulk water.

As mentioned earlier by Katti et al.[34,35] the observed change in lamellar thickness is small in comparison with the change of interlamellar spacing. This is readily seen in Figure 4, where changes in the thickness of the lamella and of the gallery are presented as functions of the applied stress. The bilayer film turns out to be more sensitive to mechanical loading; however,

TABLE 6: Calculated Estimates of the Linear CTEs of Water Layers $K^{w}_{T,Z}$ ($\times 10^{-5}$ K^{-1}) and Isothermal Compressibility β_Z of MMT Crystal and Water Layers β^{w}_{Z} (TPa^{-1}) at 300 K for Different Values h_l (nm)

	$K^{w}_{T,Z}$			β_Z	β^{w}_{Z}		
	$h_l = 0.6425$	$h_l = 0.9$	$h_l = 0.98$		$h_l = 0.6425$	$h_l = 0.9$	$h_l = 0.98$
monolayer of water	1.9	2.5	3.3	12.8	19	28	34
bilayer of water	4.5	6.0	7.0	16.2	23	30	34
water in bulk[68]	8.5			NA	150		

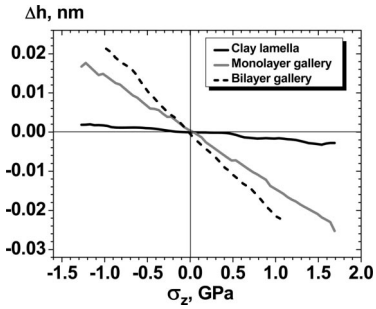

Figure 4. Changes in the thickness Δh of lamella and gallery for mono- and bilayer systems under loading along the Z axis.

TABLE 7: Comparison of the Elastic Constants (GPa) of the Hydrated MMT Crystal, Water Layer, and Clay Lamella for $h_l = 0.9$ nm

	hydrated MMTcrystal				
	with monolayer of water	with bilayer of water	clay lamella	water monolayer	water bilayer
E_1	182	150	216	90	47
E_2	180	152	233	34	24
E_3	78.1	61.7	165	32	31
E_4	20.4	2.3	44	8	1
E_5	19	4	40	8	2
E_6	66.7	56.5	84	20	14

the coefficient of isothermal compressibility, β_Z, is similar to that for the monolayer film (Table 6).

Like the coefficients of elasticity, the compressibilities for the MMT crystal are similar at $T = 300$ and 350 K. Boek et al. previously calculated the isothermal compressibility of the water layer β_Z^w from volume fluctuations.[11] Our calculation shows that compressibilities of the mono- and bilayers are also similar; however, the values of the coefficient of isothermal compressibility turn out to be somewhat larger at 58 TPa^{-1}. Despite the magnitudes of $K_{T,Z}^w$ and β_Z^w for different h_l in Table 6 being rather different, the regularities mentioned above are valid for all cases.

Similar to the calculations of $K_{T,Z}^w$ and β_Z^w, the stress and strain in the hydrated MMT crystal model can be related to the stress and strain in the individual clay lamellae and water films as follows:

$$d\sigma_i^M = h_w\sigma_i^w + h_l\sigma_i^l \quad i = 1,2,6$$
$$d\varepsilon_i^M = h_w\varepsilon_i^w + h_l\varepsilon_i^l \quad i = 3,4,5 \qquad (3)$$

where the superscripts M, w, and l refer to the hydrated MMT crystal, the interlamellar water layer, and the clay lamella, respectively. d is the layer spacing; h_l and h_w are the thickness of the interlamellar water layer and the clay lamella, respectively.

Notice that the relations in eq 3 imply that the interlamellar water layer behave as an elastic solid. From eq 3, we determine for the elastic constants of this interlamellar water layer

$$h_w E_i^w = dE_i^M - h_l E_i^l \quad I = 1,2,3$$
$$E_i^w/h_w = \frac{1}{d/E_i^M - h_l/E_i^l} \quad I = 3,4,5$$

It is seen from the results of calculations that the transverse shear of the water film determines the stiffnesses of the MMT crystal (Table 7; we present here the results for $h_l = 0.9$ nm only). The decrease of transverse shear modulus by 1 order of magnitude in the case of the water bilayer suggests a qualitative change in water structure. At the same time the significant discrepancy between in-plane elastic constants E_1 and E_2 of water interlayer, which remains invariable for the both thicknesses, most likely reflects a strong sensitivity to small differences.

6. Conclusion

The main objective of our simulation was to calculate the thermomechanical properties of the hydrated Na^+-MMT crystal. For the first time, we present the detailed MD study of the CTE and all components of the elasticity tensor of the tactoid. Results are presented for hydrated crystals at 300 and 350 K with either mono- or bilayers of water in the interlamellar galleries. The in-plane thermomechanical behavior of the clay−water/cation composite depends on the linear CTEs of the clay lamella and the thickness of the interlamellar gallery. The water layers alter significantly the linear CTE in the direction perpendicular to the plane of the lamellae, $K_{T,Z}$, which nearly triples in the case of the water bilayer. And at the same time, the coefficient $K_{T,Z}$ in the case of water monolayer was only slightly larger than that for the pyrophyllite.

An increase in the water film thickness from one to two layers led to a 20% increase in the interlamellar distance and, as a consequence, to corresponding decreases in stiffnesses. The analysis of properties of the water−cation interlamellar layer has shown that the linear CTEs of the monolayer and bilayer films are roughly one-third and two-thirds, respectively, of experimental value for bulk water. In contrast to the CTE, the coefficients of isothermal compressibility of the monolayer and bilayer films are identical and equal to approximately 3.6×10^{-11} Pa^{-1}, which is a quarter of that for water.

The calculation of all components of the elasticity tensor has shown that the tactoid possesses orthotropic symmetry. In addition, mechanical properties were practically invariable in the temperature range 300−350 K. The calculated in-plane Young's moduli of hydrated MMT, E_1, and E_2, are approximately 180 GPa for the case of a water monolayer and 150 GPa for that of a bilayer. The transversal modulus E_3 is noticeably lower, at 78 and 62 GPa for the cases of mono- and bilayer water, respectively. Transverse shear moduli decrease from 20 GPa for the water monolayer to 2−4 GPa for the bilayer. Such a significant decrease of these moduli, as well as the significant increase in $K_{T,Z}$ for the bilayer, indicate that the water interlayer transforms from solidlike to liquidlike behavior with increasing thickness.

Acknowledgment. The study was sponsored by the CRDF (Project RUC2-2626-MO-04).

References and Notes

(1) Breen, C; Thompson, G; Webb, M. *J. Mater. Chem.* **1999**, *9*, 3159.
(2) Pinnavaia, T. J.; Beall, G. W. *Polymer-Clay Nanocomposites*; John Wiley and Sons: Chichester, UK, 2000.
(3) Alcoutlabi, M.; McKenna, G. B. *J. Phys.: Condens. Matter.* **2005**, *17*, R461.
(4) Hussain, F.; Hojjati, M.; Okamoto, M.; Gorga, R. E. *J. Comp. Mater.* **2006**, *40*, 1511.
(5) Brindley, G. W.; Brown, G. *Crystal Structures of Clay Minerals and Their X-ray Identification*; Mineralogical Society: London, 1980.
(6) Skipper, N. T.; Refson, K.; McConnell, J. D. C. *J. Chem. Phys.* **1991**, *94*, 7434.
(7) Skipper, N. T.; Soper, A. K.; McConnell, J. D. C. *J. Chem. Phys.* **1991**, *94*, 5751.
(8) Skipper, N. T.; Chang, F.-R. C.; Sposito, G. *Clays Clay Miner.* **1995**, *43*, 285.
(9) Skipper, N. T.; Sposito, G.; Chang, F.-R.C. *Clays Clay Miner.* **1995**, *43*, 294.
(10) Chang, F.-R. C.; Skipper, N. T.; Sposito, G. *Langmuir* **1995**, *11*, 2734.

(11) Boek, E. S.; Coveney, P. V.; Skipper, N. T. *J. Am. Chem. Soc.* **1995**, *117*, 12608.
(12) Chang, F.-R.C.; Skipper, N. T.; Spasito, G. *Langmuir* **1995**, *11*, 2734.
(13) de Siqueira, A. V. C.; Skipper, N. T.; Coveney, P. V.; Boek, E. S. *Mol. Phys.* **1997**, *92*, 1.
(14) Smith, D. E. *Langmuir* **1998**, *14*, 5959.
(15) Shroll, R. M.; Smith, D. E. *J. Chem. Phys.* **1999**, *111*, 9025.
(16) Ichikawa, Y.; Kawamura, K.; Nakano, M.; Kitayama, K.; Kawamura, H. *Eng. Geology* **1999**, *54*, 21.
(17) Chang, F.-R.; Skipper, N. T.; Refson, K.; Greathouse, J. A.; Sposito, G. *ACS Symposium Series 715*; American Chemical Society: Washington, DC, **1999**; p 88.
(18) Park, S.-H.; Sposito, G. *J. Phys. Chem. B* **2000**, *104*, 4642.
(19) Young, D. A.; Smith, D. E. *J. Phys. Chem. B* **2000**, *104*, 9163.
(20) Chávez-Páez, M; Workum, V. K.; de Pablo, L.; de Pablo, J. J. *J. Chem. Phys.* **2001**, *114*, 1405.
(21) Charvez-Perz, M.; de Pablo, L.; de Pablo, J. J. *J. Chem. Phys.* **2001**, *114*, 10948.
(22) Hensen, E. J. M.; Tambach, T. J.; Bliek, A.; Smit, B. *J. Chem. Phys.* **2001**, *115*, 3322.
(23) Hensen, E. J. M.; Smit, B. *J. Phys. Chem. B* **2002**, *106*, 12664.
(24) Sutton, R.; Sposito, G. *Geochem. Trans.* **2002**, *3*, 73.
(25) Marry, V.; Turq, P.; Cartailler, T.; Levesque, D. *J. Chem. Phys.* **2002**, *117*, 3454.
(26) Marry, V.; Turq, P. *J. Phys. Chem. B* **2003**, *107*, 1832.
(27) Ichikawa, Y.; Kawamura, K.; Fujii, N.; Nattavut, T. *Int. J. Numer. Meth. Eng.* **2002**, *54*, 1717.
(28) Ichikawa, Y.; Kawamura, K.; Fujii, N.; Nattavut, T. *Eng. Comp.* **2003**, *20*, 559.
(29) Tambach, T. J.; Hensen, E. J. M.; Smit, B. *J. Phys. Chem. B* **2004**, *108*, 7586.
(30) Whitley, H. D.; Smith, D. E. *J. Chem. Phys.* **2004**, *120*, 5387.
(31) de Pablo, L.; Chavez, M. L.; Sum, A. K.; de Pablo, J. J. *J. Chem. Phys.* **2004**, *120*, 939.
(32) Boulet, P.; Coveney, P. V.; Stackhouse, S. *Chem. Phys. Let.* **2004**, *389*, 261.
(33) Malikova, N.; Marry, V.; Dufreche, J.-F.; Simon, C.; Turq, P.; Giffaut, E. *Mol. Phys.* **2004**, *102*, 1965.
(34) Katti, D. R.; Schmidt, S. R.; Ghosh, P.; Katti, K. S. *Clays Clay Miner.* **2005**, *53*, 171.
(35) Schmidt, S.; Katti, D. R.; Ghosh, P.; Katti, K. S. *Langmuir* **2005**, *21*, 8069.
(36) Smith, D. E.; Wang, Y.; Chaturvedi, A.; Whitley, H. D. *J. Phys. Chem. B* **2006**, *110*, 20046.
(37) Malikova, N.; Cadéne, A.; Marry, V.; Dubois, E.; Turq, P. *J. Phys. Chem. B* **2006**, *110*, 3206.
(38) Suter, J. L.; Coveney, P. V.; Greenwell, H. C.; Thyveetil, M. A. *J. Phys. Chem. C* **2007**, *111*, 8248.
(39) Porion, P.; Michot, L. J.; Faugere, A. M.; Delville, A. *J. Phys. Chem. C.* **2007**, *111*, 5441.
(40) Arab, M.; Bougeard, D.; Smirnov, K. S. *Phys. Chem. Chem. Phys.* **2004**, *6*, 2446.
(41) Wang, J. W.; Kalinichev, A. G.; Kirkpatrick, R. J. *J. Phys. Chem. B* **2005**, *109*, 14308.
(42) Leng, Y.; Cummings, P. T. *J. Chem. Phys.* **2006**, *124*, 74711.
(43) Leng, Y. S.; Cummings, P. T. *J. Chem. Phys.* **2006**, *125*, 104701.
(44) Wang, J. W.; Kalinichev, A. G.; Kirkpatrick, R. J. *Geochim. Cosmochim. Acta* **2006**, *70*, 562.
(45) Kalinichev, A. G.; Wang, J. W.; Kirkpatrick, R. *J. Cement Conc. Res.* **2007**, *37*, 337.
(46) Brodholt, J; Wood, B. *J Geophys Res.* **1993**, *98*, 519.
(47) Kawamura, K. *Molecular Dynamics Simulations*; Yonezawa, F., Ed.; Springer-Verlag: Berlin, 1992; pp 88−97.
(48) Hill, J.-R.; Sauer, J. *J. Phys. Chem.* **1994**, *98*, 1238.
(49) Hill, J.-R.; Sauer, J. *J. Phys. Chem.* **1995**, *99*, 9536.
(50) Teppen, B. J.; Rasmussen, K.; Bertsch, P. M.; Miller, D. M.; Schäfer, L. *J. Phys. Chem. B* **1997**, *101*, 1579.
(51) Boyd, S. A.; Sheng, G. Y.; Teppen, B. J.; Johnston, C. J. *Environ. Sci. Technol.* **2001**, *35*, 4227.
(52) Manevitch, O. L.; Rutledge, G. C. *J. Phys. Chem. B* **2004**, *108*, 1428.
(53) Cygan, R. T.; Liang, J. J.; Kalinichev, A. G. *J. Phys. Chem. B* **2004**, *108*, 1255.
(54) Kirkpatrick, R. J.; Kalinichev, A. G.; Hou, X.; Struble, L. *Mater. Struct.* **2005**, *38*, 449.
(55) Braterman, P. S.; Cygan, R. T. *Am. Mineral.* **2006**, *91*, 1188.
(56) Kalra, A.; Parks, D. M.; Rutledge, G. C. *Macromolecules* **2007**, *40*, 140.
(57) Mazo, M. A.; Manevitch, L. I.; Gusarova, E. B.; Shamaev, M. Yu.; Berlin, A. A.; Balabaev, N. K.; Rutledge, G. C. *J. Phys. Chem. B.* **2008**, *112*, 2964.
(58) Mazo, M. A.; Manevitch, L. I.; Gusarova, E. B.; Shamaev, M. Yu.; Berlin, A. A.; Balabaev, N. K.; Rutledge, G. C. *J. Phys. Chem. B.* **2008**, *112*, 3597.
(59) Wardle, R.; Brindley, G. W. *Am. Mineral.* **1972**, *57*, 732.
(60) Cornell, W. D.; Cieplak, P.; Bayly, C. L. *J. Am. Chem. Soc.* **1995**, *117*, 5179.
(61) Jorgensen, W. L.; Chandrashekar, J.; Madura, J. D.; Impey, R.; Klein, M. L. *J. Chem. Phys.* **1983**, *79*, 926.
(62) Berendsen, H. J. C.; Postma, J. P. M.; van Gunsteren, W. F.; DiNola, A.; Haak, J. R. *J. Chem. Phys.* **1984**, *81*, 3684.
(63) Lemak, A. S.; Balabaev, N. K. *J. Comput. Chem.* **1996**, *17*, 1685.
(64) Allen, M. P.; Tildesley, D. J. *Computer Simulation of Liquids*; Clarendon Press: Oxford, UK, 1987.
(65) Fu, M. H.; Zhang, Z. Z.; Low, P. F. *Clays Clay Miner.* **1990**, *38*, 485.
(66) Cases, J. M.; Bérend, I.; Besson, G.; Francois, M.; Uriot, J. P.; Thomas, F.; Poirier, J. E. *Langmuir* **1992**, *8*, 2730.
(67) Calvet, R. *Ann. Agron.* **1973**, *24*, 77.
(68) Nye, J. F. *Physical Properties of Crystals*; Oxford University Press: London, 1957.
(69) Chen, B.; Evans, J. R.G. *Script Mater.* **2006**, *54*, 1581.
(70) Kell, G. S. *J. Chem. Eng. Data* **1975**, *20*, 97.

JP711188U